Corrosion Behavior of Flame Sprayed Cr_2O_3 Coatings on Carbon Steel in Chloride Solutions*

*Howard Nuñez Celis***
*Mauricio Rincón Ortiz****
*Andrés Giovanni González Hernández*****

Received: 13/06/2021 • Accepted: 14/11/2021
https://doi.org/10.22395/rium.v21n40a9

ABSTRACT

Cr_2O_3 coatings were deposited on carbon steel through the flame spraying technique using two types of flames (neutral and oxidizing). The protective and morphological characteristics of the coatings were determined. The coatings had layer thickness values of 114 and 214µm for oxidizing and neutral samples, respectively. Porosity percentages of 4.5 % and 2.5 % were determined, where the neutral sample presented the greatest porosity due to the insufficient fusion of the oxide particles during the process, resulting in the formation of a heterogeneous and less compact layer. Microcracks and pores were found on the surface and cross-section of the coatings, due to the thermal expansion generated during the solidification process. The coating protective capacity was evaluated by electrochemical techniques over 672 hours in a 3.5 %wt NaCl saline solution. The results evidenced that the coatings manufactured with the oxidizing flame presented more corrosion resistance compared to those prepared with the neutral flame. The corrosion products were more evident in the neutral flame coatings, because of the diffusion mechanisms from the substrate to the surface coating through the interconnected pores. Finally, the wettability of the sodium chloride solution in the Cr_2O_3 coatings was measured by the contact angle technique, finding that the oxidizing flame coatings exhibited a higher angle contact value (64.8°) in contrast to the neutral flame coatings (35°).

Keywords: Cr_2O_3; corrosion; microstructure; flame spray; coatings; corrosion products; kinetic; polarization resistance; defects; chloride.

* Articulo derivado de la investigación realizada en el Grupo de Investigación en Desarrollo y Tecnología de Nuevos Materiales (GIMAT), la cual fue financiada con fondos de la Vicerrectoría de Investigación y Extensión (VIE) de la Universidad Industrial de Santander (UIS) a través del proyecto 2512.

** Ingeniero Metalúrgico, Grupo de Investigación en Desarrollo y Tecnología de Nuevos Materiales (GIMAT), Universidad Industrial de Santander (UIS) Cra 27 calle 9, Bucaramanga-Colombia. Correo electrónico: howard.nunez@correo.uis.edu.co, Orcid: https://orcid.org/0000-0002-3176-9782

*** Doctor en Ciencia y Tecnología Mención Materiales, Grupo de Investigación en Desarrollo y Tecnología de Nuevos Materiales (GIMAT), Universidad Industrial de Santander (UIS) Cra 27 calle 9, Bucaramanga-Colombia. Correo electrónico: mrincono@saber.uis.edu.co, Orcid: https://orcid.org/0000-0001-9977-1443

**** Doctor en Ingeniería, Grupo de Investigación en Desarrollo y Tecnología de Nuevos Materiales (GIMAT), Universidad Industrial de Santander (UIS) Cra 27 calle 9, Bucaramanga-Colombia. Correo electrónico: aggonzal@uis.edu.co, Orcid: https://orcid.org/0000-0002-8946-3735

Comportamiento corrosivo de recubrimientos de Cr_2O_3 rociados térmicamente sobre acero al carbono en soluciones de cloruro

Resumen

Los recubrimientos de Cr_2O_3 fueron depositados en un acero al carbono a través de la técnica de rociado térmico, usando dos tipos de llamas (neutra y oxidante). Se determinaron las características protectoras y morfológicas de los recubrimientos. Los recubrimientos mostraron espesores de capa con valores de 114 y 214 µm para las muestras depositadas con llamas neutra y oxidante, respectivamente. Se determinaron los porcentajes de porosidad de 4,5 y 2,5 %, en donde la muestra que se depositó con la llama neutra presentó la mayor porosidad debido a una fusión insuficiente de las partículas de óxido durante el proceso, resultando en la formación de una capa menos compacta y heterogénea. Las microgrietas y los poros se encontraron en la superficie y en la sección trasversal de los revestimientos debido a la expansión térmica generada durante el proceso de solidificación. La capacidad protectora de los recubrimientos fue evaluada a partir de técnicas electroquímicas por 672 horas en una solución salina 3,5 %wt NaCl. Los resultados evidenciaron que los revestimientos elaborados con la llama oxidante presentaron una mayor resistencia a la corrosión en comparación con aquellos elaborados con la llama neutra. Los productos de corrosión fueron más evidentes en los recubrimientos con llama neutra debido a los mecanismos de difusión desde el sustrato a la superficie recubierta a través de los poros interconectados. Finalmente, la humectabilidad de la solución de cloruro de sodio en los recubrimientos de Cr_2O_3 fueron medidos por medio de la técnica de ángulo de contacto, encontrando que los revestimientos de llama oxidante mostraron un mayor ángulo de contacto (64,8 °) en contraste con los recubrimientos de llama neutra (35 °).

Palabras clave: Cr_2O_3; corrosión; microestructura; rociado térmico; recubrimientos; productos de corrosión; cinética; resistencia a la polarización; defectos; cloruro.

INTRODUCTION

Carbon steel is a material commonly used for the manufacturing of structural components in marine environments [1]. Low carbon steels are used for general applications due to their weldability and low cost [2]. It possesses exceptional mechanical properties that make it preferable as a construction material compared to other types; however, the exposure to high humidity, chloride rich salty environments and temperature variations can accelerate its degradation [3]–[5]. Marine corrosion is hostile, mainly because of the seawater high chloride concentration and low electrical resistivity. Surface coating is a surface engineering process used to achieve the desired properties of a material only on the surface without altering the core. Nowadays, the most advantageous surface protection treatment employed for carbon steel is the coating process with corrosion resistant materials [6]. Recently, ceramic coatings have been applied on the surface of the steel to improve corrosion resistance under aggressive environments such as the marine. Likewise, other options such as metallic and organic coatings have been applied, yet, they cannot be compared with the ceramic coating performance under aggressive conditions, especially at elevated temperatures [5], [7], [8]. Different techniques or processes such as the chemical vapor deposition (CVD), physical vapor deposition (PVD) and sol-gel are used for the application of ceramic coatings on metallic alloys [9]–[11].

On the other hand, thermal spraying consists of a group of coating manufacturing processes in which finely divided metallic or non-metallic materials are deposited in a molten or semi-molten condition to form a coating. Flame spraying is one of the thermal spraying techniques most widely used for thick coating because of its low cost. In this process, the feedstock material is sprayed in the flame produced at the nozzle of a spray torch oxidation of a combustible gas. The flame simultaneously heats the feedstock material to the partial or total melting and is spreaded towards the substrate, where the particle deforms to generate a splat. The stacking of multiple splats forms the coating [12], [13]. The corrosion resistance and mechanical properties of flame spraying ceramic coatings depend primarily on the microstructural features [7], [14]. The microstructures of the coatings applied through the flame spraying technique are usually inhomogeneous. This non-homogeneity is due to different defects (pores, cracks, unmelted particles, among others) generated during the manufacturing process. These defects provide a way for aggressive ions to diffuse through the coating and reach the substrate, impairing the coating performance [7], [8]. Chromium oxide (Cr_2O_3) coatings have been evaluated as possible protective ceramic coatings for different substrates and these have been found to enhance their corrosion and wear properties [15]. Furthermore, Cr_2O_3 coatings exhibit an excellent protective capacity on metal exposed to acid and high chloride concentration environments [16]. Generally, these

are used in marine industries as corrosion resistant materials on different components [14]. Given that the melting temperature of chromium oxide, which is around 2435 °C, plasma spray has been the most utilized thermal spray process to deposit these coatings, however, it is expensive due to the procedure parameters. In recent years, ceramic coatings with a high melting point such as carbides and oxides have been produced by flame spraying, with promising protective results against aggressive environments, high temperatures, and wear conditions [17]–[20].

In this paper, chromium oxide coatings were obtained through the flame spraying technique by using two different flames on carbon steel substrates. Moreover, the protective capacity of these coatings was assessed by electrochemical techniques in chloride solutions under various exposure times at room temperature. The results of different coatings were correlated with the microstructural characteristics such as porosity, microcracks and interfacial defects to evaluate whether the proposed chromium coatings could be used in structural components exposed to marine environments.

1. MATERIALS AND METHODS

MEC 707™ (Metallizing Equipment Co.) was used to fabricate the coatings through flame spraying. This powder is composed of chromium oxide (Cr_2O_3). The phases, particle size distribution and morphology of the feedstock powder were determined by X-Ray Diffraction (XRD), Laser Diffraction and Scanning Electron Microscopy (SEM). The XRD pattern was recorded with a D8 ADVANCE BRUKER diffractometer operating in DaVinci geometry. Master Sizer 2000 equipment and QUANTA FEG 650 microscope were used to evaluate the particle size distribution and the morphology of the powder, respectively.

AISI-SAE 1020 steel bars of 25.4 mm in diameter and 8 mm thickness were used as the substrates. These were blasted with corundum jet particles to eliminate oxides and other impurities, in addition to providing an arithmetic average roughness (Ra) higher than 5 μm. This roughness is required to ensure the sprayed particles good adhesion when they reach the substrate. The average particle size for corundum was 610μm. Subsequently, the substrates were cleaned with ethanol in an ultrasonic bath to remove the residues from the surface preparation. Optical Emission Spectrometry (OES) using a Bruker Magellan Q8 was used to verify the chemical composition of the substrate.

Chromium oxide coatings were manufactured by oxy-fuel thermal spraying with a neutral (almost stoichiometric) and an oxidizing flame, using a MEC POWDER FLAME SPRAY system integrated with a POWDERJET-86-II gun, a PF-700 powder feeder, and XY Gun manipulator to control the torch movement. A mixture of 22 L/min of acetylene and 37 L/min of oxygen was used to manufacture the coatings with a neutral

flame, while 22 L/min of acetylene was mixed with 70 L/min of oxygen to produce the oxidizing flame. In all cases, the acetylene and oxygen pressures were 0.10 and 0.34 MPa, respectively. Feedstock powders were injected into the flame at a rate of 21 g/min, using 15 L/min of nitrogen as the carrier gas with the pressure of 0.13 MPa. The substrates were located 90 mm in front of the torch. While the surface of the substrates was preheated at 300 °C employing two (2) passes with the torch, the powders were sprayed for three (3) passes, all of that using a torch speed of 50 mm/s. Additionally, an air jet at a pressure of 0.13 MPa was applied with the flame to accelerate melted or semi-molten particles toward the substrate. Accordingly, the codes assigned to the samples were (N1) to the neutral and (O1) to the oxidizing flame.

The thickness of the coatings was assessed along with their cross-section was assessed by analyzing the images obtained through scanning electron microscopy (QUANTA FEG 650). The ASTM E2109 standard was used to determine the coating porosity [21]. Finally, the surface roughness of the coating was determined using a commercial rugometer.

The protective capacity of the coatings was studied in a 3.5 %wt NaCl aqueous electrolyte using a GAMRY Interface 1000™ Potentiostat/Galvanostat. The potentiostat was connected to three electrochemical cell electrodes. Saturated calomel electrode (SCE), platinum wire and the coated samples were used as the reference, counter and working electrodes, respectively. The electrochemical measurements were made by exposing 1 cm^2 of the coated surface sample to brine. Electrochemical Impedance Spectroscopy (EIS) tests were carried out according to the ASTM G106-89 standard [22]. An alternating current (AC) signal amplitude of 10 mV was applied with a frequency range between 10 kHz and 0.001 Hz. The tests were completed at the corrosion potential while exposing the coated surfaces to salt water during 24, 168, 336, 504, and 672 h. The EC-LAB™ software was used for data analysis. The samples were polarized from −300 mV to +300 mV versus open circuit potential (OCP), with a scan rate of 0.167 mV/s. The parameters needed to calculate corrosion rates were determined with the Tafel Extrapolation Method. The experiments were performed in triplicate. Additionally, the surface interaction of the coatings to a saline solution was evaluated through the measuring of the contact angle. The system for measuring the contact angle was based on the Dataphysics OCA 15 EC video, where a 3.5 wt% NaCl solution with a drop rate of 0.10 µL/s was used as the liquid.

2. RESULTS AND DISCUSSION

2.1 Material characterization

The chemical composition of the substrate was determined by Optical Emission Spectrometry (OES). The results indicated that the material used in this study corresponds

to a low carbon steel with 0.21 %wt. C, 0.56 %Mn, 0.002 %S, 0.21% Si 0.009 %P and iron. On the other hand, the powder used for the fabrication of the coatings on the carbon steel was characterized, as seen in Figure 1. SEM image of the Cr_2O_3 powders exhibited an irregular shape particle, with some fracture marks and without agglomeration as shown in Figure 1a. The XRD powder phase analysis revealed a crystalline phase of Cr_2O_3 (Eskolaite), Figure 1c. The irregular shape particles with rounded edges are owned to the manufacturing process by fracture and wear caused between them, which is characteristic of the autogenous milling process [23]. Figure 1b shows the particle size distribution of the feedstock powder used with parameters of d_{10}=13.6 µm, d_{50}= 26.7 µm and d_{90}=51.8 µm. Particle size plays a crucial role on their melting in the flame, then on the homogeneity and corrosion resistance of the coating [24].

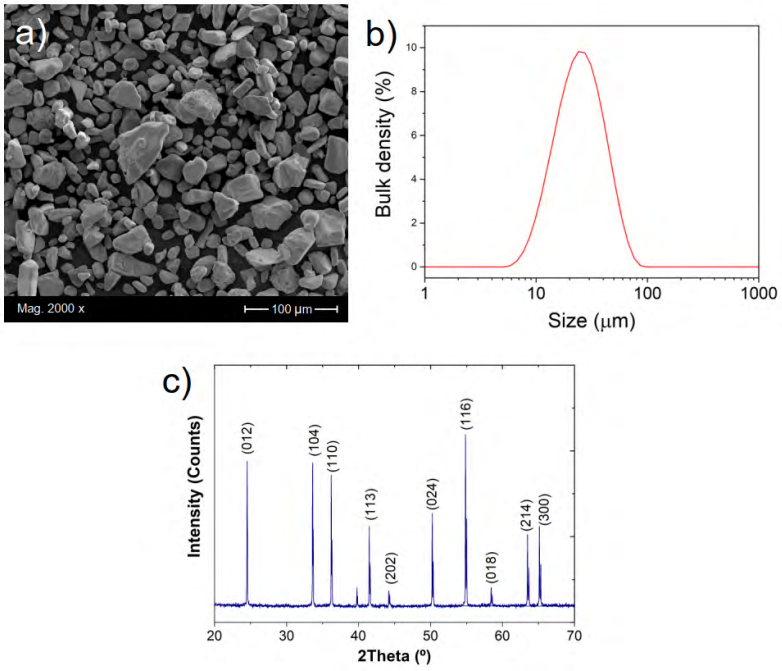

Figure 1: Powder and coating characterization: (a) SEM micrograph of Cr_2O_3 powder (b) Particle size determined by the Laser Diffraction technique (c) XRD patterns of Cr_2O_3 powder and coating.

Source: own elaboration

2.2 Microstructure of coatings

Figure 2 presents typical cross-sectional and surface morphologies of coatings elaborated by thermal spraying. The cross-sectional morphology is characterized by microcracks (included at the inner boundaries), pores, and lamellas (Figure 2a and 2c). The cross-sectional analysis of the Cr_2O_3 coating obtained under

oxidizing conditions (sample O1, Figure 2a) shows that it is relatively denser than the coating elaborated under neutral conditions (sample N1, Figure 2c). Moreover, the thickness values obtained in the samples O1 and N1 were close to 114 and 214 μm, respectively, as presented in Figures 2a and 2c. These figures clearly show that the thickness of the coating in sample N1 is greater in contrast to sample O1. In sample N1, the neutral flame reaches the highest temperature with a primary zone of shorter length, which has the hottest zone in the flame, and is not able to melt a large number of particles. On the contrary, the oxidizing flame has a larger primary zone which allows a longer travel or residence time of the particles within the flame, making them able to melt in a greater particle quantity, generating flattened lamellas in the sample O1 [25]. This is the main reason sample O1 thickness is less compared to sample N1, resulting in a denser structure. This is also reflected in the porosity measurement where the O1 coating (2.5 ± 1 %) presented a smaller porosity percentage than the N1 coating (4.5 ± 0.4 %), making sample O1 slightly denser than the N1 sample.

On the other hand, Figures 2b and 2d show the surface of the O1 and N1 coatings, respectively. The "splats" are a typical structure on the surface of the coating which can present internal microcracks as shown in Figures 2b and 2d. Those splats are the output of the rapid solidification of the molten or semi-molten droplets which impinge on a substrate. The coating is built up by successive impingement and inter-bonding among the "splats" [26]. It is important to note that the sample N1 surface has a greater number of cracks within the splats compared to sample O1, and this can affect the behavior of the coating to the permeation of an aggressive solution leading to an increase in the substrate degradation rate.

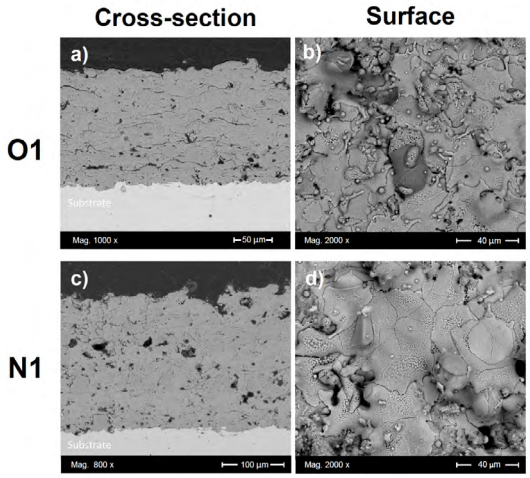

Figure 2: Morphology of the surface and cross-section coatings: (a-b) O1 (c-d) N1.

Source: own elaboration

2.3 Electrochemical corrosion tests

2.3.1 EIS analysis at different times

The EIS results obtained from Cr_2O_3 samples in the electrolyte 3.5 %NaCl solution at room temperature, are presented as Nyquist and Bode plots in Figures 3 and 4, respectively. The experiments were conducted after 24, 168, 336, 504, and 672 hours of exposure. The EIS coating plots were simulated by the equivalent circuit models shown in Figure 5. Figure 5a shows the equivalent circuit model has been previously used in different studies to fit the EIS data of ceramic coatings deposited by thermal spray and tested in chloride solutions [7], [15], [27]. The model consists of the solution resistance (R_{sol}), the pore resistance (R_{pore}), the charge transfer resistance (R_c) and constant phase elements (CPE_1 and CPE_2). The polarization resistance (R_p) parameter was defined as the sum between the R_{pore} and R_c. This parameter is proportional to the protective capacity of the coatings. CPE_1 and CPE_2 are described as an imperfect capacitor and depict the electrolyte-coating and coating-substrate interface, respectively [15], [28]. Equally, simple equivalent circuits were fitted to the carbon steel (CS) experimental data to achieve the polarization resistance (R_P), as shown in Figure 5b.

The CPE impedance is expressed by Equation 1:

$$Z_{CPE} = Q^{-1}(j\omega)^{-\alpha} \quad (1)$$

Where *j* is the imaginary unit, Q is the CPE constant, ω is the angular frequency (rad/s) and α is the CPE exponent index [15], [28], [29]. This equation can describe the impedance of a pure capacitor C for a Q=C condition and exponent α =1. For the case where α =0, the equation describes the impedance response of an ideal resistor with Q=R [15], [30]. If α =0.5, it is indicative of a diffusion controlled process that is feasible to find in coatings with high porosity [31]. Many authors have used CPE for the deviations of an ideal resistor and capacitor in response to different physical phenomena, such as inhomogeneity and surface roughness, which are commonly present in the microstructure of ceramic coatings [7], [8], [15], [27], [28], [32], [33].

Figure 3a, 3b and 3c shows the influence of the exposure time on the electrochemical impedance response of the Cr_2O_3 coatings and carbon steel (uncoated) evaluated in sodium chloride solutions. A short capacitive loop appears in the high frequencies zone of the coated samples followed by a large one at low frequencies. The semi-circle loop at the higher frequency is caused mainly by solution resistance while at lower frequency by capacitance. A Nyquist spectra trend was found showing an increase in the Rp values over time. This parameter (Rp) is proportional to the corrosion resistance and is represented by a semicircle in the section of impedance at low frequencies. However, a slight decrease in Rp with the exposure time was evidenced for the O1

and N1 specimens after meeting the maximum values 5857.9 ± 121 Ωcm^2 at 336 h and 2059.4 ± 159 Ωcm^2 at 504 h of exposure time respectively, indicative of corrosion resistance loss of the coatings, which could have resulted due to the detachment from corrosion products of the coating surfaces. The differences of polarization resistance values between O1 and N1 samples are mainly attributed to the degree of permeability in the coatings by the type of flame employed. Likewise, it is important to underline that carbon steel (CS) exhibited a similar behavior to the N1 coatings at 672h of exposure.

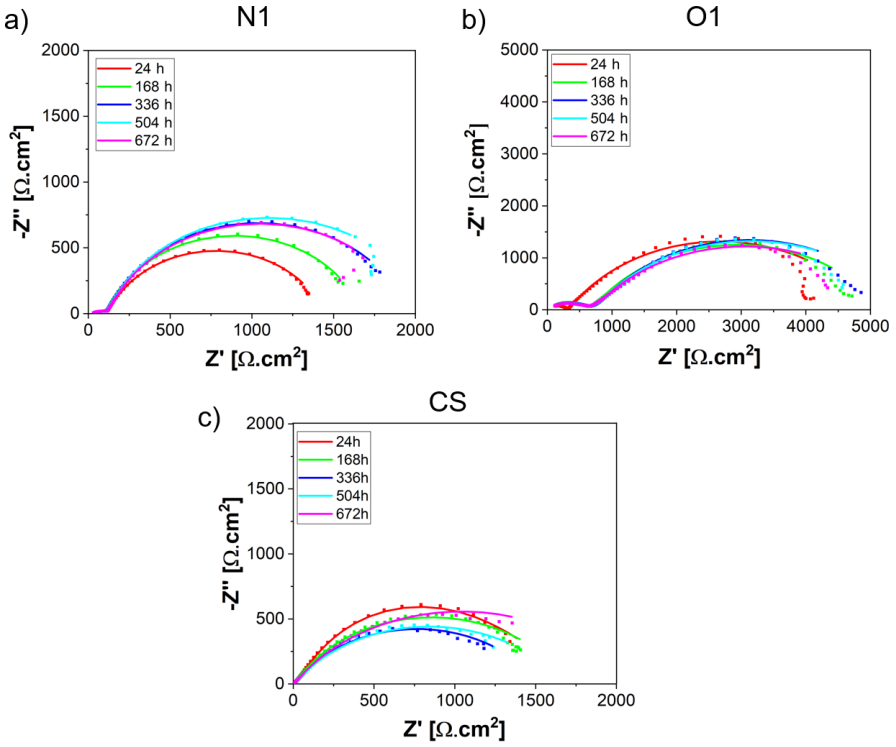

Figure 3: Nyquist plots of samples evaluated in 3.5 %wt NaCl at different immersion periods: (a) O1 (b) N1.

Source: own elaboration

The corrosion parameters obtained from fitting the data to the equivalent circuit are shown in Table 1.

Table 1: Properties of coatings and electrochemical measurements in 3.5 wt %NaCl solutions at different immersion periods.

Sample	Thickness (μm)	Porosity (%)	Time (h)	Rs (Ω.cm^2)	Rpore (Ω.cm^2)	Rc (Ω.cm^2)	Rp (Ω.cm^2)
O1	114	2.5	24	20.36	325.80	4685	5010.8
			168	70.31	708.40	4498	5206.4
			336	71.46	769.90	5088	5857.9
			504	72.30	790.40	4846	5636.4
			672	71.50	771.10	4678	5449.1
N1	214	4.5	24	27.02	102.80	1313	1415.8
			168	26.13	98.56	1547	1645.6
			336	26.04	98.00	1786	1884.0
			504	26.60	100.40	1959	2059.4
			672	27.27	103.60	1843	1946.6
CS	-	-	24	7.27	-	-	1870.3
			168	6.76	-	-	1592.4
			336	6.13	-	-	1525.1
			504	4.84	-	-	1686.4
			672	4.18	-	-	2076.2

Source: own elaboration

An alternative method for impedance data representation is the Bode plot where, log |Z| is plotted vs log ω. Figure 4 shows the Bode plots of the coatings and carbon steel for different exposure times. Z' represents the real part and Z'' means the virtual part. The impedance modulus is defined as [34]:

$$|Z| = (Z' + Z'')^{1/2} \quad (2)$$

At a low frequency, the maximum impedance modulus |Z| of the N1 coatings is 1912 ± 42 Ωcm^2 at 504 h and the minimum value is 1420 ± 38 Ωcm^2 at 24 hours of exposure in the brine solution. Similarly, for the O1 coatings values of |Z| around 4863 ± 56 Ωcm^2 and 4021 ± 65 Ωcm^2 at exposure times of 336 and 24 hours were found, respectively. Finally, the carbon steel exhibited values of maximum |Z| near of 2311 ± 73 Ωcm^2 at 24 hours and the minimum |Z| around 1269± 38 Ωcm^2 at 504 hours of exposure. Previous results validate the information found in relation to the Nyquist diagrams and the simulations conducted for the determination of the different electrochemical parameters as shown in Table 1. Otherwise, the coating microstructure is crucial in the performance of protection capacity due to the compacting and porosity percentage, which is directly controlled by the flame and spraying distance used. Likewise, the quantity and diffusion mechanism of the corrosion products formed as a consequence of ag-

gressive ions is another phenomenon responsible for increasing the impedance value, as reported by López-Ortega et al. [3].

In addition, another method for plotting impedance data includes the phase angle δ, which is defined as [34]:

$$tan\,\delta = \frac{Z''}{Z'} \tag{3}$$

The variations of phase angles are directly related to the coating behavior in terms of the capacitance and resistance and may indicate the performance of the coatings [35]. Figure 4a shows the phase angle as a function of the frequency for the N1 coatings. A semicircular loop of 5Hz and 1mHz, with a maximum phase angle δ of (-48°) was found for the N1 coatings under exposure times of 168, 336, 504 and 672 hours. However, for a time of 24 hours, the semicircular loop exhibited a small shifting at higher frequencies with a maximum phase angle of (-42 °).

Conversely, the phase angle obtained for the O1 coatings after exposure to the electrolyte at different times is presented in Figure 4b. Two-time constants can be observed at different frequency ranges. Whereas the first constant at the high frequency is attributed to the solution resistance (Rsol) and may indicate the coating performance in a later state, the second constant at the lower frequency is associated with the coating capacitance [35], [36]. The maximum phase angle was found at 24 hours with a value about (-36 °) and a frequency range between 100 Hz and 1 mHz. For longer exposure times, δ had a stationary value of (-29 °) and a frequency range between 10 Hz and 1 mHz. This shifting and decrease in the phase angle in the direction of the lower frequency is related to the active corrosion process at the coating/solution interface and the accumulation of corrosion products, serving as a barrier for the passage of the chloride ions towards the carbon steel [36]. It is pertinent to highlight that the carbon steel exhibited the maximum phase angle δ at 672 h of exposure, owing to the increase of the corrosion products on the surface, resulting in a rise of the protective capacity of the generated layer.

While comparing the Nyquist and Bode results for the samples N1 and O1, the existence of differences in the protective mechanisms and the electrochemical behavior of the coatings can be observed, situation that, could be associated with the penetration of chloride ions, oxygen and water molecules, which lead to the formation of defects or inhomogeneities (pores, microcracks, unmelted particles, etc.) [37]. Particularly, the N1 coatings presented a more capacitive behavior, contrary to what happened with O1 coatings which showed a more resistive tendency.

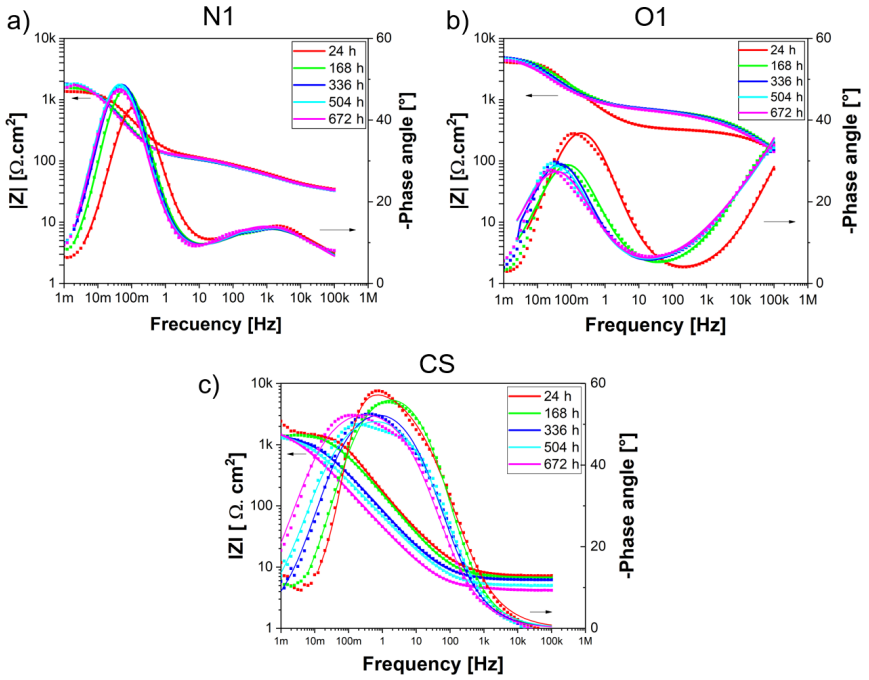

Figure 4: Bode plots of samples evaluated in 3.5 % wt NaCl at different immersion periods: (a) O1 (b) N1.

Source: own elaboration

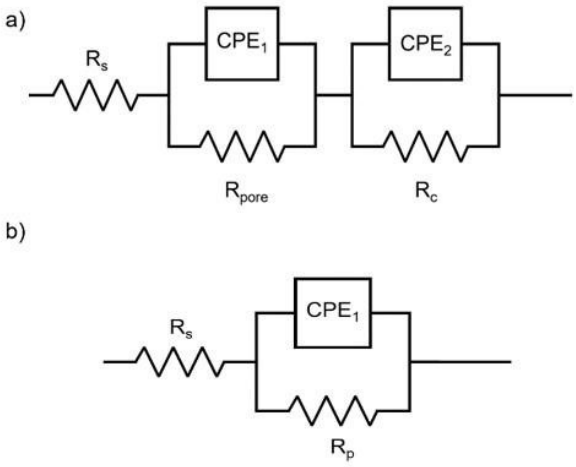

Figure 5: Equivalent circuits for metals coated by flame spraying tested in chloride solution: (a) Equivalent circuit model with two- time constants (b) Simple equivalent circuit with one time constant.

Source: own elaboration

Figure 6 shows the corrosion products generated on the surface of the O1 and N1 coatings after 672 h of immersion. The presence of corrosion products in the O1 coatings was lower compared to the N1 coatings samples, as proved in the SEM results. The EDS analysis of the corrosion products evinced mostly the presence of iron and oxygen. Sodium is shown in the EDS spectra since the coatings were exposed to NaCl solutions; however, the presence of chloride ions on the surface of the coatings was not confirmed. As for the O1 coatings, corrosion products formed on the coating surface were quite protective and surface-adhered, as seen in Figure 6a. Nevertheless, the same phenomenon did not occur for the N1 coatings, as seen in Figure 6b. The main reason for this difference in the protective capacity is because of the quantity and size of the defects present in the coatings, which are the means of transportation for the aggressive ions to reach the substrate.

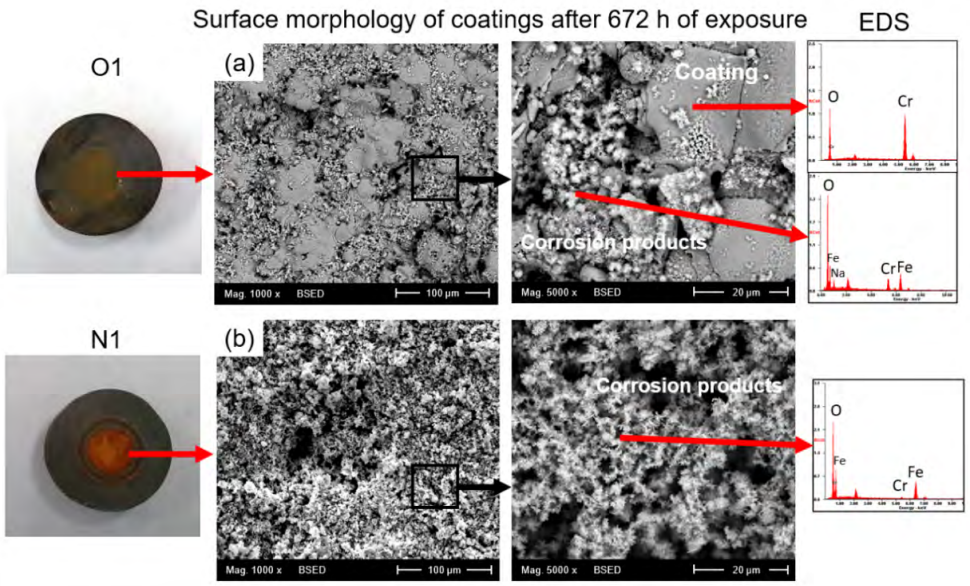

Figure 6: Surface morphology and EDS analysis of Cr_2O_3 coatings after 672 h of exposure in 3.5 % wt NaCl. (a) O1 (b) N1.

Source: own elaboration

2.3.2 Tafel extrapolation method

The results obtained by potentiodynamic polarization tests after 672 h of exposure to 3.5 % wt NaCl solution for the O1 and N1 coatings, as well as CS are presented in the Tafel curves, Figure 7. Kinetic parameters such as the corrosion current density (i_{corr}) and corrosion rates (CR) were determined and listed in Table 2. The Stern-Geary relationship [38] was used to calculate the i_{corr}, as shown in Equation (4):

$$i_{corr} = \frac{\beta_A . \beta_C}{2.303 \,.\left(R_p\right).\left(\beta_A + \beta_C\right)} \tag{4}$$

Where β_A and β_C (in mV dec^{-1}) are the anodic and cathodic Tafel slope, respectively, determined with the Tafel extrapolation method, and R_p (Ω.cm^2) is the polarization resistance determined from EIS. High β_C was determined, indicating that the cathodic curves were controlled by mass transfer [34]. Based on the results, the corrosion current density (i_{corr}) of the O1 specimens showed the lowest i_{corr} after 672 h of exposure, in contrast to those observed for the N1 samples, meaning that the former protects more efficiently the carbon steel substrate from the different stages of the corrosive process.

By means of Faraday's Law [39] and in accordance with the ASTM G-102-89 [40] standard, the corrosion rate (mmpy) was calculated as:

$$CR = \frac{EW \;.k\;.\; i_{corr}}{\rho} \tag{5}$$

Where EW is the equivalent weight =27.94 g/eq, (k) is the faradaic constant with a value of 3.27 x 10^{-3} mm g/µA cm year, i_{corr} is the corrosion current density and ρ the carbon steel density (7.87 g/cm^3).

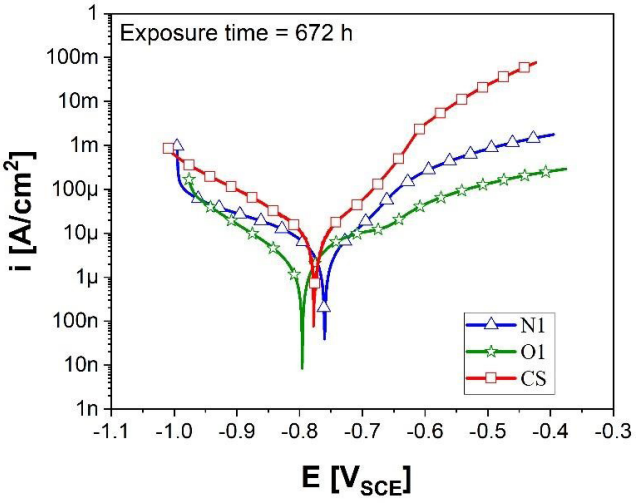

Figure 7: Potentiodynamic curves obtained for Cr_2O_3 coatings and carbon steel after 672 h of exposure in 3.5 %wt NaCl.

Source: own elaboration

The lowest corrosion rate was obtained for the O1 samples with a value of 0.05 mm/year which was almost four times lower compared to the N1 samples (CR = 0.18 mm/year). Likewise, this corrosion rate value for the O1 specimens is much alike to those reported in the literature for hard chromium coatings exposed to saline

solutions [7], [41]. The highest corrosion rates for the N1 coatings are primarily attributed to the number of interconnected pores in the microstructure. However, these values are similar in comparison with the corrosion rate values determined for non-coated carbon steel.

Table 2: Parameters obtained by the Tafel extrapolation method of coated specimens in 3.5 %wt NaCl solutions

Sample	β_A (mV/dec)	β_C (mV/dec)	i_{corr} (μA/ cm²)	CR (mm/year)
O1	99.40	106.50	4.10	0.05
N1	68.14	170.12	10.85	0.12
CS	89.86	133.14	11.22	0.13

Source: own elaboration

2.4 Contact angle measurement

The results of the contact angle measurement are shown in Figure 8, where Figure 8(a) and (b) present samples N1 and O1, respectively. Contact angle measurement appears to be a functional approach to understand the effect of chemical compositions of solid surfaces on wettability [42]. Accordingly, the contact angle of the samples N1 and O1 was less than 90 °, demonstrating that both surfaces have a hydrophilic behavior indicative of a partial wetting [43]. In general, coatings with larger angles are typically more protective against metal corrosion [44]. Comparing both samples, the sample O1 exhibited a higher angle value (64.8 °) than sample N1 (35 °). Likewise, roughness values were obtained for coatings O1 (15.13 μm) and N1 (17.57 μm) specimens, respectively. This property can be associated with the type of morphology and roughness of the surface of the coatings, which correlates to the type of flame (neutral and oxidizing) used to elaborate the coatings. Noticeably, the interaction between the saline solution and the surface generates a greater contact angle in the sample O1, which can be explained due to the presence of well-fused splats with a high degree of flatness resulting in a lower surface roughness. In contrast, the splats with a low melting degree in the coating were mainly presented in the specimen elaborated by the neutral flame (sample N1), producing a low contact angle. Moreover, the effect of this greater contact angle between sample O1 with respect to sample N1, can be compared in the same way with the better corrosion resistance presented in sample O1. One approach to understand this behavior is that considering there was less contact between the surface of the coating (sample O1) and the saline solution, this reduced the permeation of chloride ions through the coating. For that reason, the better corrosion resistance of sample O1 can be influenced by the interaction between its surface and the saline solution, since this sample showed a higher contact angle.

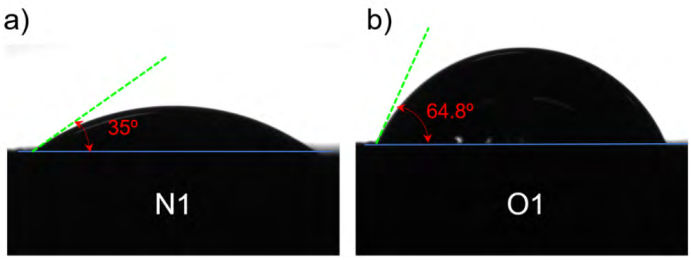

Figure 8: Contact angle for Cr_2O_3 coatings in 3.5 wt% NaCl: (a) N1 (b) O1.

Source: own elaboration

3. CONCLUSIONS

- Oxidizing and neutral flames were used to elaborate two Cr_2O_3 coating types through oxyacetylene flame spraying. The oxidizing flame generated more compact coatings with an average thickness of 114 μm and porosity percentages of 2.5 %. This behavior is due to the higher thermal energy provided to the particles from the oxidizing flame owing to longer flight time within the flame, which results in greater fusion. At the same time, the lowest viscosity achieved in the more molten particles produces flatter and then thinner lamellar structures together with a more compact surface arrangement.

- The coating with the better behavior and protective capacity was obtained with the oxidizing flame, reaching corrosion rates of 0.05 mmpy, approximately three times lower than those elaborated with the neutral flame. This accomplishment is acquired since its structure is more compact and has less number of pores and microcracks, which produced a layer of higher resistance to the initiation of corrosion processes from the transport of chloride ions into the microstructure of the coating.

- Finally, the microstructure obtained through the oxidizing flame coating showed a measured contact angle average of 64.8 °, being higher than those made with the neutral flame (35 °). Consequently, this coating could achieve a lower contact between the solution and the surface due to its microstructure, a fact that was demonstrated in its better corrosion resistance.

ACKNOWLEDGEMENTS

The authors gratefully appreciate Universidad Industrial de Santander-VIE, Colombia, for the financial support of project No. 2512, titled *"Evaluación de la microestructura, propiedades mecánicas y resistencia a la corrosión de recubrimientos de Cr_2O_3 y Cr_2O_3-Al_2O_3 elaborados a partir de proyección térmica por combustión para aplicaciones en ambientes marinos"*.

REFERENCES

[1] A. López-Ortega, J. L. Arana, E. Rodríguez, and R. Bayón, "Corrosion, wear and tribocorrosion performance of a thermally sprayed aluminum coating modified by plasma electrolytic oxidation technique for offshore submerged components protection," *Corros. Sci.*, vol. 143, pp. 258–280, Oct. 2018, doi: 10.1016/j.corsci.2018.08.001.

[2] D. Dwivedi, K. Lepková, and T. Becker, "Carbon steel corrosion: a review of key surface properties and characterization methods," *RSC Adv.*, vol. 7, no. 8, pp. 4580–4610, 2017, doi: 10.1039/C6RA25094G.

[3] A. López-Ortega, R. Bayón, and J. L. Arana, "Evaluation of protective coatings for offshore applications. Corrosion and tribocorrosion behavior in synthetic seawater," *Surf. Coatings Technol.*, vol. 349, pp. 1083–1097, Sep. 2018, doi: 10.1016/j.surfcoat.2018.06.089.

[4] Y. Ma, Y. Li, and F. Wang, "Corrosion of low carbon steel in atmospheric environments of different chloride content," *Corros. Sci.*, vol. 51, no. 5, pp. 997–1006, May 2009, doi: 10.1016/j.corsci.2009.02.009.

[5] B. Syrek-Gerstenkorn, S. Paul, and A. J. Davenport, "Use of thermally sprayed aluminium (TSA) coatings to protect offshore structures in submerged and splash zones," *Surf. Coatings Technol.*, vol. 374, no. April, pp. 124–133, 2019, doi: 10.1016/j.surfcoat.2019.04.048.

[6] K. V. Sreenivas Rao, G. C. Tejaswini, and K. G. Girisha, "Corrosion Behavior of Plasma Sprayed Cr2O3 - Al2O3 - ZrO2 Multilayer Coatings on Mild Steel," 2018, doi: 10.1016/j.matpr.2018.10.200.

[7] A. V. Pinzón, K. J. Urrego, A. González-Hernández, M. Rincón Ortiz, and F. Vargas Galvis, "Corrosion protection of carbon steel by alumina-titania ceramic coatings used for industrial applications," *Ceram. Int.*, vol. 44, no. 17, 2018, doi: 10.1016/j.ceramint.2018.08.273.

[8] Z. Liu, Y. Dong, Z. Chu, Y. Yang, Y. Li, and D. Yan, "Corrosion behavior of plasma sprayed ceramic and metallic coatings on carbon steel in simulated seawater," *Mater. Des.*, vol. 52, no. 29, pp. 630–637, 2013, doi: 10.1016/j.matdes.2013.06.002.

[9] A. S. Hamdy, D. P. Butt, and A. A. Ismail, "Electrochemical impedance studies of sol-gel based ceramic coatings systems in 3.5% NaCl solution," *Electrochim. Acta*, vol. 52, no. 9, pp. 3310–3316, 2007, doi: 10.1016/j.electacta.2006.10.036.

[10] X. Huang, S. Sun, and G. Tu, "Investigation of mechanical properties and oxidation resistance of CVD TiB2 ceramic coating on molybdenum," *J. Mater. Res. Technol.*, vol. 9, no. 1, pp. 282–290, 2020, doi: 10.1016/j.jmrt.2019.10.056.

[11] J. Lawal, P. Kiryukhantsev-Korneev, A. Matthews, and A. Leyland, "Mechanical properties and abrasive wear behaviour of Al-based PVD amorphous/nanostructured coatings," *Surf. Coatings Technol.*, vol. 310, pp. 59–69, 2017, doi: 10.1016/j.surfcoat.2016.12.031.

[12] P. L. Fauchais, J. V. R. Heberlein, and M. I. Boulos, *Thermal spray fundamentals: From powder to part*. 2014.

[13] V. R. S. Sá Brito, I. N. Bastos, and H. R. M. Costa, "Corrosion resistance and characterization of metallic coatings deposited by thermal spray on carbon steel," *Mater. Des.*, vol. 41, pp. 282–288, Oct. 2012, doi: 10.1016/j.matdes.2012.05.008.

[14] P. Zamani and Z. Valefi, "Microstructure, phase composition and mechanical properties of plasma sprayed Al2O3, Cr2O3 and Cr2O3-Al2O3 composite coatings," *Surf. Coatings Technol.*, vol. 316, pp. 138–145, 2017, doi: 10.1016/j.surfcoat.2017.03.022.

[15] A. M. Oje, A. A. Ogwu, S. U. Rahman, A. I. Oje, and N. Tsendzughul, "Effect of temperature variation on the corrosion behaviour and semiconducting properties of the passive film formed on chromium oxide coatings exposed to saline solution," *Corros. Sci.*, vol. 154, no. April, pp. 28–35, 2019, doi: 10.1016/j.corsci.2019.04.004.

[16] P. S. Babu, D. Sen, A. Jyothirmayi, L. R. Krishna, and D. S. Rao, "Influence of microstructure on the wear and corrosion behavior of detonation sprayed Cr2O3-Al2O3 and plasma sprayed Cr2O3 coatings," *Ceram. Int.*, vol. 44, no. 2, pp. 2351–2357, 2018, doi: 10.1016/j.ceramint.2017.10.203.

[17] F. Fanicchia, D. A. Axinte, J. Kell, R. McIntyre, G. Brewster, and A. D. Norton, "Combustion Flame Spray of CoNiCrAlY & YSZ coatings," *Surf. Coatings Technol.*, vol. 315, pp. 546–557, 2017, doi: 10.1016/j.surfcoat.2017.01.070.

[18] A. Förg, M. Blum, A. Killinger, J. A. Moreno Nicolás, and R. Gadow, "Deposition of chromium oxide-chromium carbide coatings via high velocity suspension flame spraying (HVSFS)," *Surf. Coatings Technol.*, vol. 351, no. July, pp. 171–176, 2018, doi: 10.1016/j.surfcoat.2018.07.072.

[19] X. B. Liang, J. C. Shang, Y. X. Chen, Z. D. Zhou, Z. B. Zhang, and B. S. Xu, "Influence of ceramic particles and process parameters on residual stress of flame-sprayed Fe-based coatings," *Surf. Coatings Technol.*, vol. 354, no. August, pp. 10–17, 2018, doi: 10.1016/j.surfcoat.2018.08.069.

[20] R. Rachidi, B. El Kihel, and F. Delaunois, "Microstructure and mechanical characterization of NiCrBSi alloy and NiCrBSi-WC composite coatings produced by flame spraying," *Mater. Sci. Eng. B Solid-State Mater. Adv. Technol.*, vol. 241, no. November 2017, pp. 13–21, 2019, doi: 10.1016/j.mseb.2019.02.002.

[21] ASTM International, "ASTM E2109−01: Test Methods of Determining Area Percentage Porosity in Thermal Sprayed Coatings," *Stand. Test Methods Determ. Area Percent. Porosity Therm. Sprayed Coatings*, vol. 01, no. Reapproved 2014, pp. 1–8, 2014, doi: 10.1520/E2109-01R14.2.

[22] ASTM G 106, "Standard Practice for Verification of Algorithm and Equipment for Electrochemical Impedance Measurements," *Astm*, vol. 03, no. Reapproved, pp. 1–11, 1999, doi: 10.1520/G0106-89R10.2.

[23] S. K. Sriramoju, Rashmi, A. Suresh, and P. S. Dash, "Generation of low ash fine clean coal powder by autogenous grinding process powder technology," *Powder Technol.*, vol. 342, pp. 67–72, 2019, doi: 10.1016/j.powtec.2018.09.079.

[24] N. H. N. Yusoff, M. J. Ghazali, M. C. Isa, A. R. Daud, and A. Muchtar, "Effects of powder size and metallic bonding layer on corrosion behaviour of plasma-sprayed Al2O3-13% TiO2 coated mild steel in fresh tropical seawater," *Ceram. Int.*, vol. 39, no. 3, pp. 2527–2533, 2013, doi: 10.1016/j.ceramint.2012.09.012.

[25] E. C. Iglesias, C. P. Velásquez, and F. V. Galvis, "Estudio de llamas oxiacetilénicas usadas en la proyección térmica," no. 9, pp. 15–26, 2016.

[26] E. E. Balić, M. Hadad, P. P. Bandyopadhyay, and J. Michler, "Fundamentals of adhesion of thermal spray coatings: Adhesion of single splats," *Acta Mater.*, vol. 57, no. 19, pp. 5921–5926, 2009, doi: 10.1016/j.actamat.2009.08.042.

[27] F. Vargas, H. Ageorges, P. Fauchais, M. E. López, and J. A. Calderon, "Permeation of saline solution in Al2O3-13wt.% TiO2 coatings elaborated by atmospheric plasma spraying," *Surf. Coatings Technol.*, vol. 220, pp. 85–89, 2013, doi: 10.1016/j.surfcoat.2012.11.038.

[28] S. K. Singh, S. P. Tambe, G. Gunasekaran, V. S. Raja, and D. Kumar, "Electrochemical impedance study of thermally sprayable polyethylene coatings," *Corros. Sci.*, vol. 51, no. 3, pp. 595–601, 2009, doi: 10.1016/j.corsci.2008.11.025.

[29] S. L. De Assis, S. Wolynec, and I. Costa, "Corrosion characterization of titanium alloys by electrochemical techniques," *Electrochim. Acta*, vol. 51, no. 8–9, pp. 1815–1819, 2006, doi: 10.1016/j.electacta.2005.02.121.

[30] V. F. ILvovich, *Impedance spectroscopy: Applications to Electrochemical and Dielectric Phenomena*. New Jerdey: Wiley, 2012.

[31] A. K. Basak, J. P. Celis, P. Ponthiaux, F. Wenger, M. Vardavoulias, and P. Matteazzi, "Effect of nanostructuring and Al alloying on corrosion behaviour of thermal sprayed WC-Co coatings," *Mater. Sci. Eng. A*, vol. 558, pp. 377–385, 2012, doi: 10.1016/j.msea.2012.08.015.

[32] F. Shao, K. Yang, H. Zhao, C. Liu, L. Wang, and S. Tao, "Effects of inorganic sealant and brief heat treatments on corrosion behavior of plasma sprayed Cr2O3-Al2O3 composite ceramic coatings," *Surf. Coatings Technol.*, vol. 276, pp. 8–15, 2015, doi: 10.1016/j.surfcoat.2015.06.045.

[33] C. Haixiang and K. Dejun, "Comparison on electrochemical corrosion performances of arc and laser thermal sprayed Al–Ti–Ni coatings in marine environment," *Mater. Chem. Phys.*, vol. 251, no. January, p. 123200, 2020, doi: 10.1016/j.matchemphys.2020.123200.

[34] E. McCafferty, *Introduction to corrosion science*, Springer. Alexandria VA: Springer, 2010.

[35] Y. Zuo, R. Pang, W. Li, J. P. Xiong, and Y. M. Tang, "The evaluation of coating performance by the variations of phase angles in middle and high frequency domains of EIS," *Corros. Sci.*, vol. 50, no. 12, pp. 3322–3328, 2008, doi: 10.1016/j.corsci.2008.08.049.

[36] H. S. Lee, J. K. Singh, and J. H. Park, "Pore blocking characteristics of corrosion products formed on Aluminum coating produced by arc thermal metal spray process in 3.5 wt.% NaCl solution," *Constr. Build. Mater.*, vol. 113, pp. 905–916, 2016, doi: 10.1016/j.conbuildmat.2016.03.135.

[37] Z. Bergant, U. Trdan, and J. Grum, "Effect of high-temperature furnace treatment on the microstructure and corrosion behavior of NiCrBSi flame-sprayed coatings," *Corros. Sci.*, vol. 88, pp. 372–386, 2014, doi: 10.1016/j.corsci.2014.07.057.

[38] M. Stern and A. . Geary, "Electrochemical polarization; I. Polarization curves," *J. Electrochem.*, vol. 104, pp. 56–63, 1957.

[39] S. . Dean, W. . France, and S. . Ketcham, *"Electrochemical Methods" Hanbook on Corrosion Testing and Evaluation*. New York: John Wiley, 1971.

[40] ASTM G102-89, "Standard Practice for Calculation of Corrosion Rates and Related information from Electrochemical Measurements," *ASTM*, pp. 1–7, 2015.

[41] X. Wang, B. Lv, Z. Hu, and B. Xu, "Corrosion resistance in sodium chloride solution of Ni-Co-P electro-brush amorphous coatings to replace hard chromium coatings," *Phys. Procedia*, vol. 50, no. October 2012, pp. 191–198, 2013, doi: 10.1016/j.phpro.2013.11.031.

[42] T. S. Hamidon and M. H. Hussin, "Susceptibility of hybrid sol-gel (TEOS-APTES) doped with caffeine as potent corrosion protective coatings for mild steel in 3.5 wt.% NaCl," *Prog. Org. Coatings*, vol. 140, no. November 2019, p. 105478, 2020, doi: 10.1016/j.porgcoat.2019.105478.

[43] Y. M. Liu, Z. Q. Wu, and D. C. Yin, "Measurement of contact angle under different gravity generated by a long-arm centrifuge," *Colloids Surfaces A Physicochem. Eng. Asp.*, vol. 588, no. December 2019, p. 124381, 2020, doi: 10.1016/j.colsurfa.2019.124381.

[44] N. Karthik, S. Asha, and M. G. Sethuraman, "Influence of pH-sensitive 4-aminothiophenol on the copper corrosion inhibition of hybrid sol–gel monolayers," *J. Sol-Gel Sci. Technol.*, vol. 78, no. 2, pp. 248–257, 2016, doi: 10.1007/s10971-015-3944-5.